SPi | Journal Code: J G R B | Article ID 5 1 4 0 4 | Dispatch: 04.12.15 | CE: AMI | No. of Pages: 19 | ME:

AGU PUBLICATIONS

JGR

Journal of Geophysical Research: Solid Earth

RESEARCH ARTICLE

10.1002/2015JB012023

Key Points:
- We computed new GPS velocities in the peri-Adriatic area
- Eurasia is deforming and rotating clockwise between the Alps and the Aegean
- We test whether gravity could lead the deformation in Apennines and Albanides

Supporting Information:
- Table S1
- Table S2
- Table S3
- Text S1, Figures S1–S12, and Tables S1–S3

Correspondence to:
M. Métois,
marianne.metois@ingv.it

Citation:
Métois, M., N. D'Agostino, A. Avallone, N. Chamot-Rooke, A. Rabaute, L. Duni, N. Kuka, R. Koci, and I. Georgiev (2015), Insights on continental collisional processes from GPS data: Dynamics of the peri-Adriatic belts, *J. Geophys. Res. Solid Earth*, *120*, doi:10.1002/2015JB012023.

Received 9 MAR 2015
Accepted 19 NOV 2015
Accepted article online 23 Nov 2015

Insights on continental collisional processes from GPS data: Dynamics of the peri-Adriatic belts

M. Métois[1], N. D'Agostino[1], A. Avallone[1], N. Chamot-Rooke[2], A. Rabaute[3], L. Duni[4], N. Kuka[4], R. Koci[4], and I. Georgiev[5]

[1]Istituto Nazionale di Geofisica e Vulcanologia, Centro Nazionale Terremoti, Rome, Italy, [2]Laboratoire de Géologie, Ecole Normale Supérieure, Paris, France, [3]GEOSUBSIGHT-ISTeP-UMR 7193 UPMC-CNRS, Université Pierre et Marie Curie, Paris, France, [4]Institute of Geosciences, Polytechnic University of Tirana, Tirana, Albania, [5]National Institute of Geophysics, Geodesy and Geography, Sofia, Bulgaria

Abstract We present a new GPS velocity field covering the peri-Adriatic tectonically active belts and the entire Balkan Peninsula. From the velocities, we calculate consistent strain rate and interpolated velocity fields. Significant features of the crustal deformation include (1) the eastward motion of the northern part of the Eastern Alps together with part the Alpine foreland and Bohemian Massif toward the Pannonian Basin, (2) shortening across the Dinarides, (3) a clockwise rotation of the Albanides-Hellenides, and (4) a southward motion south of 44°N of the inner Balkan lithosphere between the rigid Apulia and Black Sea, toward the Aegean domain. Using this new velocity field, we derive the strain rate tensor to analyze the regional style of the deformation. Then, we devise a simple test based on the momentum balance equation, to investigate the role of horizontal gradients of gravitational potential energy in driving the deformation in the peri-Adriatic tectonically active mountain belts: the Eastern Alps, the Dinarides, the Albanides, and the Apennines. We show that the strain rate fields observed in the Apennines and Albanides are consistent with a fluid, with viscosity $\eta \sim 3 \times 10^{21}$ Pa s, deforming in response to horizontal gradients of gravitational potential energy. Conversely, both the Dinarides and Eastern Alps are probably deforming in response to the North and North-East oriented motion of the Adria-Apulia indenter, respectively, and as a consequence of horizontal lithospheric heterogeneity.

1. Introduction

The surface deformation in collisional belts has challenged the plate tectonics theory for a long time. Indeed, most mountain belts and in particular the Himalayas and the Andes are characterized by broad deforming areas with multiple active faults far from the simple view of a sharp boundary between two large and rigid lithospheric plates [e.g., *Molnar*, 1988; *Molnar and Tapponnier*, 1975]. In the last decades, several attempts to model these complex deformation patterns have been conducted based on different assumptions about the rheology of the lithosphere and the forces affecting it. First, several authors proposed first-order models of mountain belt deformation considering that lithosphere can be split into small-scale rigid blocks rotating around Euler poles and bounded by active faults accommodating their relative motion [e.g., *Chen et al.*, 2004; *Meade*, 2007; *Thatcher*, 2007]. However, alternative models assuming a continuous and viscous lithosphere deforming under kinematics boundary conditions and body forces have been shown to reproduce just as well the deformation in these areas [e.g., *Flesch et al.*, 2000; *Vergnolle et al.*, 2007; *Copley*, 2008]. Indeed, the horizontal gradients of gravitational potential energy (GPE) between mountain ranges and their forelands [e.g., *Molnar and Lyon-Caen*, 1988; *England and Houseman*, 1989; *England and Molnar*, 1997], together with lateral variations in the lithosphere rheology [e.g., *Robl and Stüwe*, 2005; *Copley*, 2008], may be controlling a significant part of the continental deformation. Based on mantle anisotropy and surface velocity measurements, it has also been proposed that astenospheric convective motions could drive surface deformation through basal shearing of the lithosphere [e.g., *Le Pichon and Kreemer*, 2010; *Brun and Sokoutis*, 2010]. Overall, determining which of these mechanisms (boundary conditions, body forces, elastic loading on active faults, and mantle-driven deformation) is dominant and controls the deformation pattern in a continental mountain belt is not a simple problem [see *Thatcher*, 2009, for a review]. Here we take advantage of a new velocity field covering the deforming peri-Adriatic region and the Balkan Peninsula to assess whether the peri-Adriatic belts are deforming as a consequence of horizontal GPE gradients or if other controlling factors may play a role.

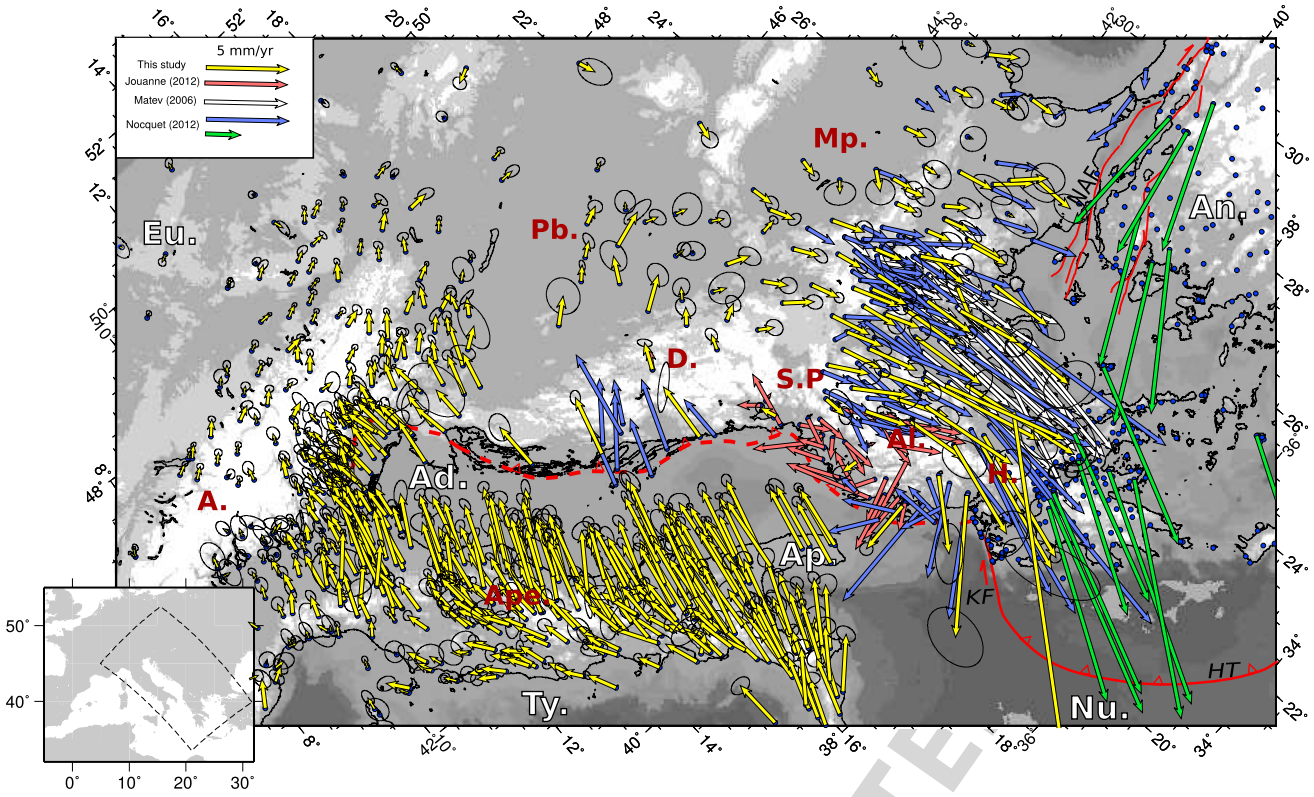

Figure 1. Tectonic context and velocity field. Velocity of the Italian and Balkan Peninsulas in our new Eurasia-fixed reference frame. Yellow arrows: new velocities processed in this study together with their 80% confidence ellipses; pink, white, and blue arrows: velocities from *Jouanne et al.* [2012], *Matev* [2011], and *Nocquet* [2012], respectively, rotated in our reference frame; green arrows: few of the many velocities available in highly deforming Greece and Turkey (see additional supporting information for the full data set used here) plotted with a different scale. Uncertainties are not plotted for clarity purpose. Red bold lines: main tectonic structures. NAF: North Anatolian Fault, HT: Hellenic Thrust, KF: Kefalonia Fault. Dotted red line: supposed position of the east Adriatic thrust. A.: Alps, Ad.: Adria block, Al.: Albanides, An.: Anatolian Plate, Ap.: Apulia block, Ape.: Apennines, D.: Dinarides, Eu.: stable Eurasia, H.: Hellenides, Mp.: Moesian platform, Nu.: Nubian Plate, Pb.: Panonnian Basin, S.P.: Scutari-Peck transform zone, Ty.: Tyrrhenian Sea.

Our study area, namely, the peri-Adriatic region, encompasses the Italian Peninsula, the Po Plain, a large part of the Central and Eastern Alps with their associated forelands, the Balkan Peninsula, and the Aegean domain. The Balkan Peninsula, i.e., the portion of Eurasia located in between the Adriatic Sea to the west and the Black Sea to the east and extending from the Alpine and Carpathian mountain belts to the north to the highly straining central Greece to the south, is certainly the less well-known part of this large region (Figure 1). Indeed, it is often considered as a stable part of the Eurasian Plate. Compared to the seismically very active zones in the vicinity of structures such as the strike-slip North Anatolian Fault (NAF) and the extensional Corinth Gulf [e.g., *Jolivet et al.*, 2013], the Balkan Peninsula is seismically relatively quiet. However, it experienced large and destructive earthquakes in the past, mainly in the vicinity of the Dinarides and Albanides mountain belts. More than eight $M_w > 6$ shallow crustal earthquakes occurred since the beginning of the twentieth century, including the 1904, M_s 7.2 Krupnik, the 1963, M_w 6.2 Skopje, and the 1979, M_w 6.9 Montenegro earthquakes [*Ambraseys and Jackson*, 1998; *Shanov and Dobrev*, 2000; *Petrovski*, 2004; *Galasso et al.*, 2013].

Over the past few years, several GPS studies brought new insights on the deformation pattern around the Adriatic Sea. First, the nearly rigid rotation of the Adria and Apulia microplates forming the core of the Adriatic domain generates a 2 to 4 mm/yr northeastward motion into the Eastern and Central Alps [e.g., *D'Agostino et al.*, 2008; *Cheloni et al.*, 2014] and into the Dinarides [e.g., *Serpelloni et al.*, 2005; *D'Agostino et al.*, 2008; *Nocquet*, 2012]. Furthermore, the eastward motion of the Eastern Alps toward the Pannonian Basin has been extensively discussed and analyzed [e.g., *Robl and Stüwe*, 2005; *Selverstone*, 2004; *Ratschbacher et al.*, 1991]. Second, very dense measurements available over the Italian Peninsula have confirmed that the Apennines are extending in a roughly SW-NE direction along their topographic crest [e.g., *D'Agostino et al.*, 2008, 2014]. Finally, in the Balkan Peninsula, the NS extension observed in Northern Greece and the Aegean Sea continues

at ~5 mm/yr into the inner Balkans and the southern margin of the Pannonian Basin [*Matev*, 2011; *Burchfiel et al.*, 2006; *Perouse et al.*, 2012]. Moreover, northwestern Greece and Albania are rotating clockwise [*Reilinger et al.*, 2010; *Nocquet*, 2012; *Perouse et al.*, 2012; *Jouanne et al.*, 2012]. Therefore, the peri-Adriatic area including the Balkans is slowly but actively deforming (Figure 1). The lack of sufficiently dense GPS measurements has prevented so far the determination of a consistent image of the peri-Adriatic domain deformation and of the transition from the SW-NE compression across the Dinarides to the NE-SW extension pattern documented in Southern Balkans [e.g., *Burchfiel et al.*, 2006; *Perouse et al.*, 2012; *Nocquet*, 2012].

Since the beginning of the 21st century, new GPS networks have been developed for scientific research but also for civilian applications (e.g., cadastral and telecommunications), in particular in the Balkans area. Here we take advantage of these continuous GPS data coming from academic and nonacademic networks to obtain a new interseismic velocity field. We calculate an interpolated velocity field and compute the homogeneous strain rate distribution over the entire area using the method described by *Haines and Holt* [1993]. The derived strain rate map brings new insights into the deformation pattern within the continental collision systems around the Adriatic Sea. Finally, we propose a simple method to test the role of gravity on the dynamics of the peri-Adriatic mountain belts. We take advantage of the new velocity field to carry out simple tests that allow us to discuss whether the deformation of the lithosphere in the region of interest is mainly controlled by forces applied at its edges, by gravitational forces or strength heterogeneities arising from horizontal heterogeneities in crustal and lithospheric structures.

2. GPS Data and Processing

In this study, we gather data from 711 permanent stations coming from scientific and civilian GPS networks distributed over the Eurasian plate, Balkan Peninsula, Greece, Italy, Turkey, and Austria together with more widely distributed stations for reference frame realization (additional supporting information). All networks made the receiver-independent exchange files directly available to us, allowing for a consistent processing for all the stations, except the Austrian network that only provides only provides solution independent exchange (*SINEX*) solutions (i.e., coordinates and their covariances, see section 2.3).

2.1. Data Processing

GPS data were reduced using the Jet Propulsion Laboratory (JPL) ~~GPS Inferred Positioning System (GIPSY) Orbit Analysis Simulation Software (OASIS)~~ II software (version 6.2) in a precise point positioning mode applied to ionospheric-free carrier phase and pseudorange data [*Zumberge et al.*, 1997] and using JPL's final fiducial-free GPS orbit products [*Bertiger et al.*, 2010]. We apply the Global Mapping Function [*Böhm et al.*, 2006] and estimate tropospheric wet zenith delay and horizontal gradients as stochastic random walk parameters every 5 min [*Bar-Sever et al.*, 1998], to model tropospheric refractivity. We compute the ocean loading from the FES2004 tidal model coefficients provided by the Ocean Tide Loading Provider [http://holt.oso.chalmers.se/loading & *Scherneck*, 1991] and apply it as a station motion model. Ambiguity resolution is applied using the wide lane and phase bias method [*Bertiger et al.*, 2010]. Finally, station coordinates obtained in the loose frame of JPL fiducial-free GPS orbits are transformed into the IGS08 reference frame [*Rebischung et al.*, 2012] using daily seven parameter transformations provided by JPL.

2.2. Eurasian Reference Frame

Because we aim at resolving small interseismic velocities (~1 mm/yr), we take a special care in realizing an accurate continental-scale reference frame. To analyze and interpret station velocities relative to the Eurasia plate with the largest possible accuracy, we have specifically built a new terrestrial reference frame for studying deformation in and around that plate following the approach of *Blewitt et al.* [2013]. This frame is defined by six Cartesian coordinates and velocities of each of 174 stations selected by specific quality criteria (Figure 2 and additional supporting information). Our frame is based on GPS time series from 2000.0 to 2014.1 obtained from daily coordinates of over 1000 GPS stations regularly processed at INGV-Rome with the GIPSY software, following the strategy presented in section 2.1. Our Eurasian frame is aligned in origin and scale with International GNSS Service 2008 (IGS08) [*Rebischung et al.*, 2012], a GPS-based realization of International Terrestrial Reference Frame 2008 (ITRF2008) [*Altamimi et al.*, 2011]. It is implemented to have no-net rotation with respect to the stable interior of the Eurasian plate, realized by a core of 69 stations (Figure 2). The Eurasia Euler pole relative to ITRF08 defined by these core stations (with a normalized root-mean-square nRMS lower than 0.3 mm/yr on each horizontal velocity component) is (−55.413°E, 81.778°N, −0.258°/Myr). Relative to

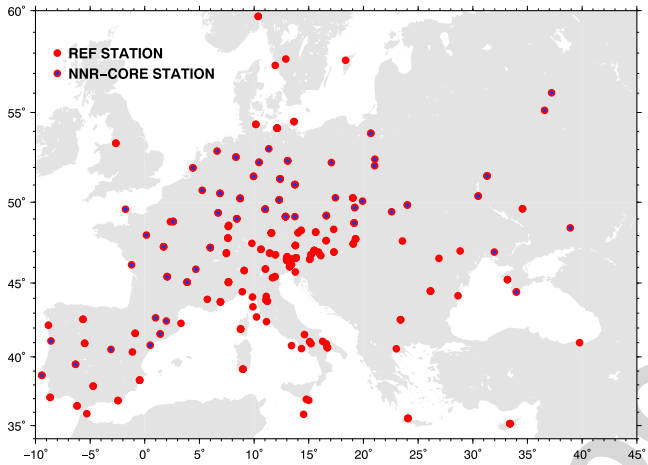

Figure 2. Permanent stations used for reference frame building. Red dots: position of permanent GPS stations used for Eurasia-fixed reference frame building; blue dots: core stations defining its no-net rotation condition.

their frame-predicted positions, the 174 frame stations have a daily RMS scatter of 1.1 mm in the north, 0.9 mm east, and 3.8 mm in the vertical (Figure S1).

This reference frame realization method transforms the station time series into a plate-fixed frame and effectively applies a continental-scale spatial filter to the station coordinates, leading to a reduction of the common-mode errors [*Wdowinski et al.*, 1997], and to an increase of the signal-to-noise ratio (Figure S2).

2.3. Integration of Austrian Coordinate Solutions

In this study we integrate our daily solutions with the ones calculated by the Space Research Institute (Austrian Academy of Sciences) and distributed by OLG (Observatory Lustbuehel Graz) at ftp://olggps.oeaw.ac.at [*Haslinger et al.*, 2007]. These solutions include the stations of the Austrian permanent GPS network APOS (http://www.bev.gv.at), together with additional stations from EUREF and IGS networks. We used the "GP5yyddd0" solutions provided in SINEX format. The original solutions are obtained using the Bernese software [*Hugentobler et al.*, 2006] following the standards of the ~~EUREF~~-EUREF Permanent Network Analysis Centers (http://www.epncb.oma.be/_productsservices/analysiscentres). To align the Austrian solutions in our realization of the Eurasian frame, we select 13 stations common to our and OLG solutions. We combine the daily OLG solutions in the period 2008.0–2014.44 of these 13 stations (BODO, BRBZ, KOE2, GRAZ, LINZ, WTZR, STBZ, PFA2, PENC, SPRN, ZIMM, STPO, and VLCH), constraining a priori their linear velocities to follow our Eurasia plate-fixed estimates. Before the combination, the covariance matrix of each daily OLG solution is augmented (i.e., "loosened") assuming large variances in the seven transformation parameters. *Blewitt* [1998] showed that this covariance augmentation procedure is equivalent to estimating a daily seven parameter transformation simultaneously with the velocities and epoch positions. We then align the original, complete OLG daily solutions to the newly calculated solution, using a seven parameters Helmert transformation. An average number of 12.6 stations were used to calculate the daily alignment of the OLG solutions. After the Helmert transformation the 13 stations have a daily RMS scatter about their frame-predicted positions of 1.1 mm in the north, 1.0 mm east, and 2.9 mm in the vertical. These values are very similar to the daily RMS scatter of the 174 stations used to realize the Eurasian reference about their frame-predicted positions (see previous section), suggesting a similar level of noise shared by the OLG solution and ours. This procedure allows us to have daily coordinates and associated covariance matrix in a Eurasian plate reference realization equivalent to the one used for our own solutions.

2.4. Velocities Estimate

We estimate interseismic long-term velocities together with annual and semiannual constituents from the continuous GPS time series using the Customer Analysis and Targeting System software [*Williams*, 2008]. We use an error model dominated by white noise plus flicker noise to estimate the associated uncertainties and remove outliers. Every time series covering more than 2.5 years (Figure S3) has been manually scrutinized to detect anomalous behavior (instrumental drifts or oscillations associated to bedrock or building instabilities) or unreferenced jumps, before estimating long-term velocities. The standard deviation is 0.61 mm for both east and north components on average.

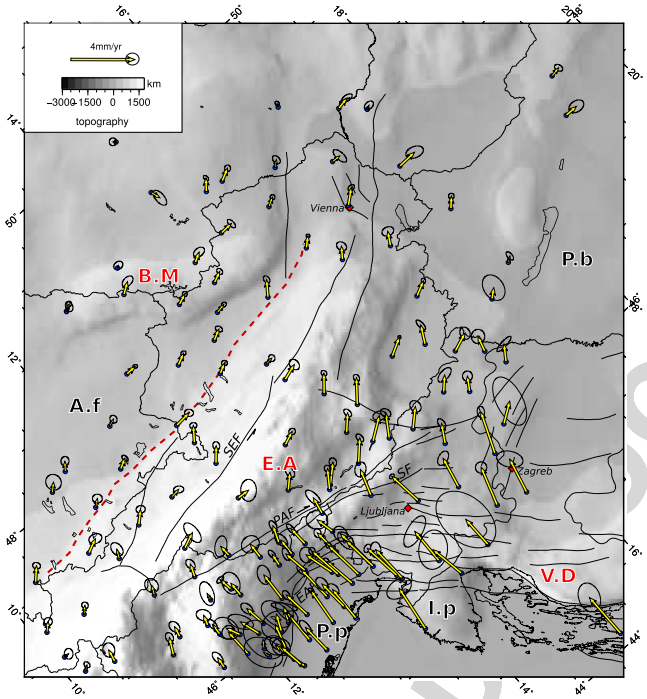

Figure 3. Kinematics of the Eastern Alps. Zoom on the velocity field presented in Figure 1 for the Eastern Alps area, plotted in our Eurasia-fixed reference frame together with filtered ETOPO1 topography. Bold black curves: main active faults taken from the SHARE catalogue (www.share-eu.org); red diamonds: main cities. A.f: Alpine foreland, P.p: Po Plain, P.b: Pannonian Basin, I.p: Istria peninsula, E.A: Eastern Alps, V.D, Velebit Dinarides; B.M, Bohemian Massif, PAF: peri-Adriatic fault, SEF: Salzach-Ennstal fault, SF: Sava Fault, EAF: eastern Alpine front. Black arrows indicate the supposed direction of the strike-slip motion on the Alpine faults. Bold dashed brown line: topographic front of the Alps.

We combine our new velocity field with previously published interseismic velocities in areas where our data is sparse, i.e., in Albania [*Jouanne et al.*, 2012], in Macedonia [*Matev*, 2011], in the Aegean domain, and along the Adriatic-Dinaric coast [*Nocquet*, 2012] after a rotation in our Eurasia-fixed reference frame. Residuals between our data set and the velocities from *Jouanne et al.* [2012] and *Nocquet* [2012] once rotated in our reference frame are lower than 0.6 mm/yr on each component (see Table S1). The final velocity field presented in Figures 1, 3, and 4 shows velocities both from campaign surveys [*Jouanne et al.*, 2012] and permanent stations, and it captures the overall consistent deformation pattern of the region. Some regions are relatively undersampled (i.e., Croatia and Bosnia), but our velocity field is sufficiently dense in Slovenia, Serbia, and Austria (SIGNAL, AGROS, and APOS networks, respectively, see additional supporting information) to display the main deformational features. The complete velocity field is available as supporting information. F3 F4

3. Deformation Pattern

3.1. Velocity Field Analysis

We observe in Figure 1 the main features of central Mediterranean tectonics: (i) the 2–4 mm/yr NE directed motion of the Adriatic region and the extension across the Apennines at about 3 mm/yr; (ii) the ~2 mm/yr shortening across the southern front of the Eastern Alps and the progressive eastward rotation of velocities toward the Pannonian Basin; (iii) the ~4 mm/yr shortening across the Dinarides; and (iv) the southward increasing motion of the Aegean domain and the Southern Balkans toward the Hellenic trench. The novelty of this velocity field described in details in the following (Figures 1, 3, and 4) lies in particular in the dense velocity fields in Serbia, Slovenia, Austria, and Macedonia illuminating the deformational features located along the actively deforming belts circling the Adriatic Sea, so far neglected in regional kinematic studies.

We image a ~4 mm/yr gradient in horizontal velocity across the Dinarides (Figure 1), but available velocities are too sparse to conclude whether this NW-SE compression is taken up by a single front or by several active structures (see profile B on Figure 5). However, it appears that this shortening is accommodated within less F5

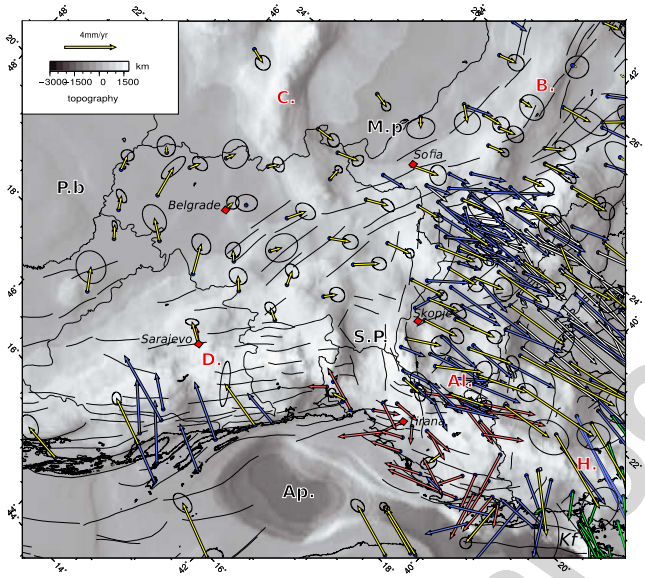

Figure 4. Kinematics of the Dinarides-Albanides area. Zoom on the velocity field presented in Figure 1 for the Dinarides-Albanides area, plotted in our Eurasia-fixed reference frame together with filtered ETOPO1 topography. The arrow color-code is the same than for Figure 1. Bold black curves: main active faults taken from the SHARE catalogue (www.share-eu.org); red diamonds: main cities. D.: Dinarides; P.b: Pannonian Basin; C.: Carpathian; B.: Balkans belt; S.P.: Scutari-Peck area; Al.: Albanides; H.: Hellenides; Ap.: Apulia. Kf: Kefalonia fault.

than ~400 km from the Adriatic coast and therefore barely propagates into the Pannonian Basin. East of the Dinarides, the north-south motion significantly increases southwards from the inner Balkans to the Aegean extensional area (see profile C in Figure 5). This overall motion of material toward the south is maximal near 23°E and decreases toward the Black Sea on the east and the Adriatic Sea on the west.

Together, the compression across the Dinarides and the extension of the southern Balkans form a clockwise rotation motion around Northern Albania (Figure 4). This rotation has been partly described by *Nocquet* [2012] and *Perouse et al.* [2012], but the lack of data in the inner Balkans prevented from a precise determination of the northward extent of the rotation cell. Our results show that the rotation propagates up to the southwestern portion of the Pannonian Basin, in Serbia (44.5°N), and develops around the Albania-Montenegro border, i.e., at the transition from the Dinarides to the Albanides mountain belts corresponding to the Scutari-Peck area (Figures 1 and 4).

The lack of data in Croatia and Bosnia prevents from obtaining the details of the deformation across the Northern Dinarides and the Istria Peninsula. However, comparison between the horizontal velocity at the station ZADA (15.228°E, 44.113°N) near the Velebit coastal range and the stations along the Slovenia-Croatia border shows that limited shortening is occurring (Figure 3). This suggests that the NE oriented Adriatic oblique motion can only be partially accommodated along the coast and may be more significantly absorbed to the North in the Sava fault area [e.g., *Vrabec and Fodor*, 2006]. Indeed, North of the Istria Peninsula, the shortening is taken up by the eastward extension in Slovenia of the Eastern Alps thrust front. Together with this small N-S gradient of horizontal velocity, we image for the first time a regional eastward rotation of the entire Slovenia which cannot be fully explained by local strike-slip motion of the easternmost sections of the peri-Adriatic fault (PAF in Figure 3).

Thanks to the dense velocity field in Austria, we image with great details the motion of the inner Eastern Alps. It clearly appears on Figure 3 that north of the Eastern Alps front and of the peri-Adriatic fault zone that experiences a ~1 mm/yr right-lateral gradient, the crust is moving eastward together with part of the Alpine foreland and the Bohemian Massif. This motion comes without any clear velocity gradient across the northern front of the Alps nor across the Salzach-Ennstal strike-slip fault that is supposed to accommodate part of the Alps escape toward the Pannonian Basin [*Selverstone*, 2004; *Ratschbacher et al.*, 1991]. In other words, there is no evidence in the GPS measurements that this strike-slip fault has a significant slip rate nor that the northern front is an active structure. Rather than localized deformation on active structures, we observe

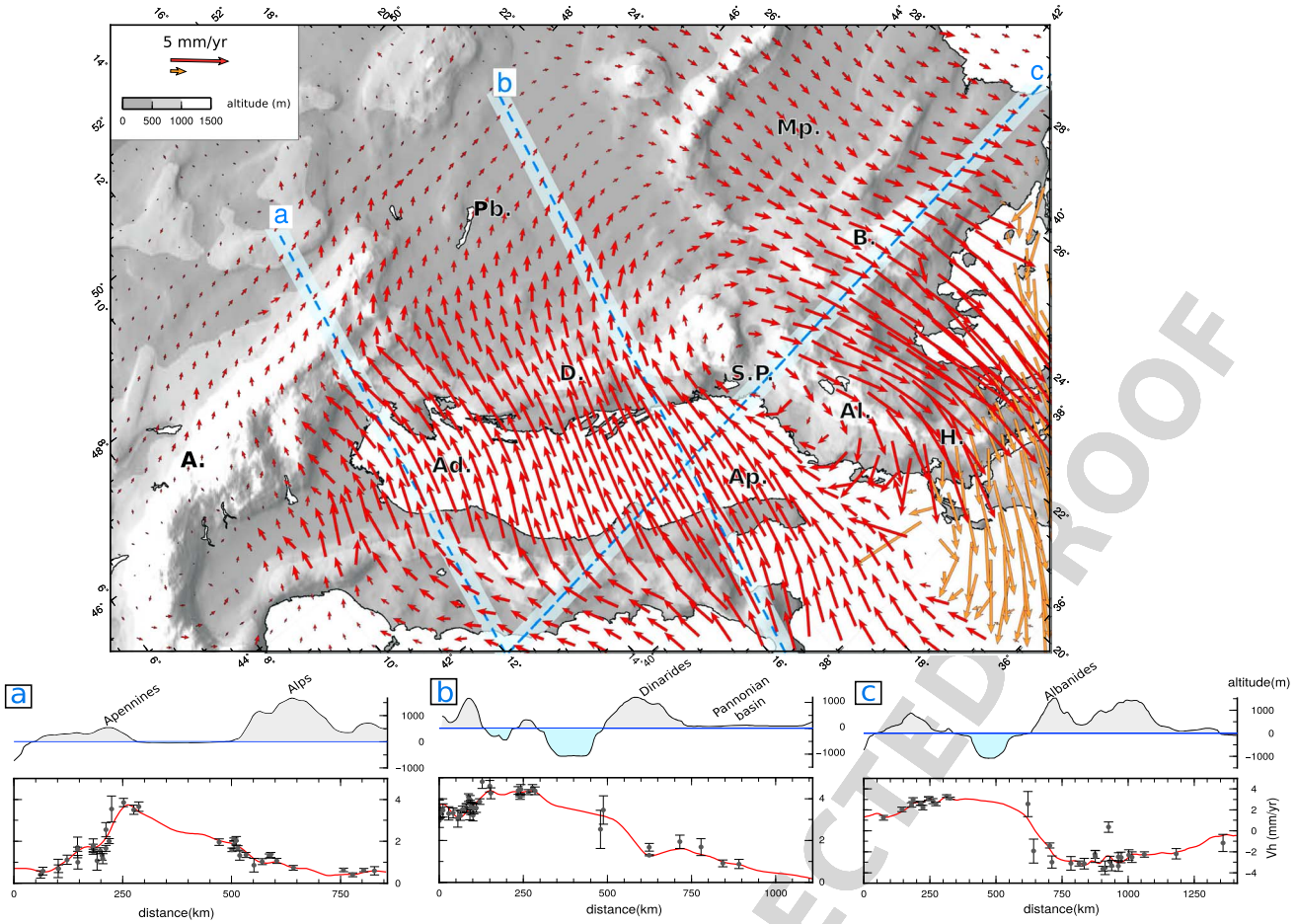

Figure 5. Interpolated velocity field. (top) Interpolated velocity field relative to stable Eurasia as defined by our new reference frame. Scale has been reduced near the Anatolia-Eurasia Plate boundary for clarity purposes (orange arrows). (bottom) Altitude (top), observed (grey dots), and interpolated (red curve) horizontal velocity projected along three 20 km width profile lines a, b, and c plotted as dashed blue lines on the map. The main geological features are indicated as in Figure 1. D. Dinarides, H. Hellenides, B. Balkan belt.

a systematic ~1 mm/yr eastward motion relative to stable Eurasia, which affects the Eastern Alps and their foreland (Figure 3).

The flow of crustal material with respect to stable Eurasia observed both in the southwestern Balkans and in the Eastern Alps can be described as a clockwise rotation around the Albanides and Slovenia. However, this rotations fundamentally differs from a rigid block motion, which would produce increasing velocities away from the Euler pole and constant velocities along small circles around the axis of rotation. None of these features applies to the velocity field of Figure 1 in these two regions (Figure S8).

3.2. Strain Rates Analysis

To compute a continuous spatial distribution of the deformation, we use the principles of continuum mechanics to analyze the strain rate tensor field. We used the *SPARSE* code provided by *Haines and Holt* [1993] to derive a continuous velocity gradient tensor field from our GPS observations, using a velocity and strain rate bicubic Bessel spline interpolation technique [*Beavan and Haines*, 2001]. SPARSE provides also estimates of strain rate and interpolated velocity for any point in our model grid. This regular grid consists in 3120 0.4° × 0.4° cells covering the area going from 8°E to 34°E and from 32.5°N to 52°N, thus including the Hellenic subduction zone and the North Anatolian Fault. We require there be no deformation inside the northernmost cells located on the stable European craton in order to mimic rigid plate behavior of the Eurasian plate (Figure S4). To avoid patchy strain rate distribution due to contradictory velocities or to observational density contrasts, we impose a smoothing parameter controlling the maximal change in slip rate values between two grid cells and fix it to 1 mm/yr since it provides a good compromise between the fit to the observed GPS velocities and the spatial

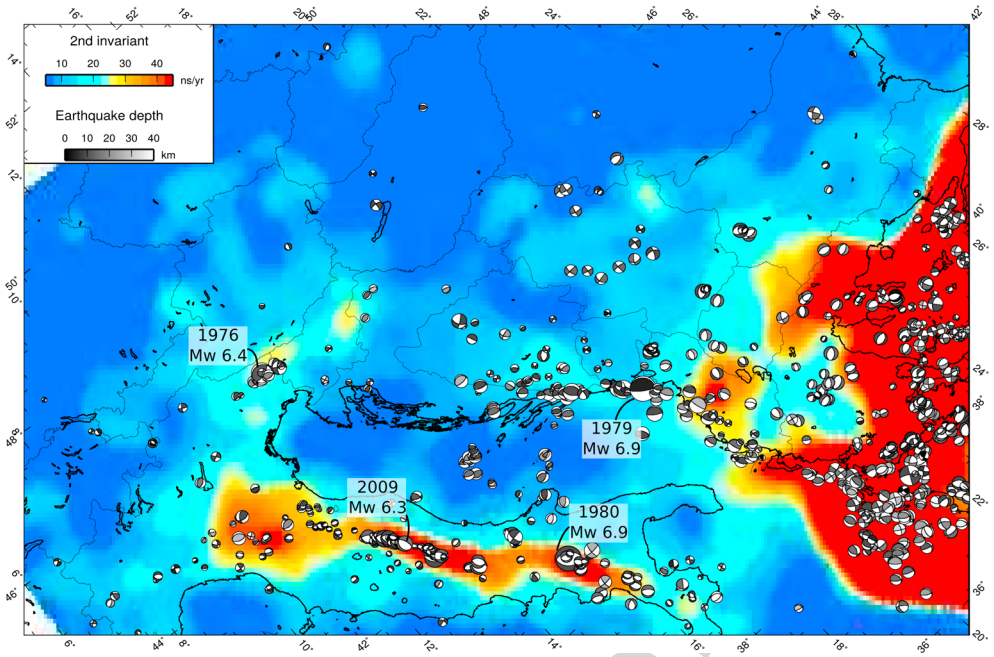

Figure 6. Map of the second invariant of the strain rate tensor over the peri-Adriatic area together with moment tensors of $M_w > 4.5$ instrumental earthquakes combined from regional *Pondrelli et al.* [2006, 2011] and global CMT and color coded depending on their epicentral depth. Time and magnitude of the largest instrumental earthquakes are indicated.

consistency of the strain rate distribution. Following *Perouse et al.* [2012], we allow cells located in the vicinity of the NAF and the Hellenic backstop to deform at higher strain rates than elsewhere in order to better retrieve the deformation associated to elastic loading on these structures.

We constrain the direction of the strain rate field to be consistent with the principal axis of deformation derived from seismic moment tensors of the Harvard centroid moment tensor (CMT) and regional CMT catalogs [*Pondrelli et al.*, 2006, 2011] (Figure 6), thus introducing strength anisotropy (Figure S5). Note that the sign and amplitude of the strain rate are left free in the inversion and that a homogeneous uniform calculation, and a more realistic model including weak zones and strength anisotropy do not significantly differ in the fit to the data in the peri-Adriatic area (nRMS is 1.46 and 1.26, respectively, Figure S7). This is probably due to the fact that this region is far from the zones under high strain and that few focal mechanisms are available there (Figure 6).

In Figure 6 we plot the second invariant of the strain rate tensor defined as $\dot{E} = \sqrt{(\dot{\epsilon}_{xx}^2 + \dot{\epsilon}_{yy}^2 + 2\dot{\epsilon}_{xy}^2)}$, $\dot{\epsilon}_{ij}$ being the ijth horizontal component of the strain rate tensor $\dot{\epsilon}$, to highlight the areas of highest strain rates. To picture the deformation patterns, Figure 7a shows the first invariant of the strain rate tensor $d = 1/2(\dot{\epsilon}_{xx} + \dot{\epsilon}_{yy})$ (for dilatation $d > 0$ and for compression $d < 0$). Figure 7b shows the vorticity of the interpolated velocity field $(\partial_x v_y - \partial_y v_x)$.

Overall, the pattern of strain around Northern Albania shown on Figures 1 and 5 is clearly delineated in Figure 6, where we observe a strain rate of $\sim 15 \times 10^{-9}$/yr in Serbia and inner Bosnia and up to 25×10^{-9}/yr on the Montenegro coast (Figure 6). Strain rate increases by a factor of 2 going from Albania and Macedonia to Northern Greece, while there is little or no straining in the Carpathians and the main part of the Pannonian Basin. In Italy, as previously shown by *D'Agostino et al.* [2014], the strain rate is the most important in the center of the Apennines mountain belt where extension is oriented SW-NE. In Slovenia, north-south compression is dominant and reaches 20 to 30×10^{-9}/yr.

The Adria and Apulia regions exhibit very low strain rates and opposite signs of vorticity, in agreement with the hypothesis of an Adriatic promontory fragmented into two rigid blocks rotating in opposite sense [*D'Agostino et al.*, 2008]. From the interpolated velocity field, we derive Euler poles best reproducing the rigid blocks motions (nRMS < 0.6). We find that the Euler poles obtained for Adria (45.69°N, 4.89°E, 0.25°/Myr) and Apulia (37.62°N, 30.94°E, −0.18°/Myr) are in good agreement with the ones determined in previous

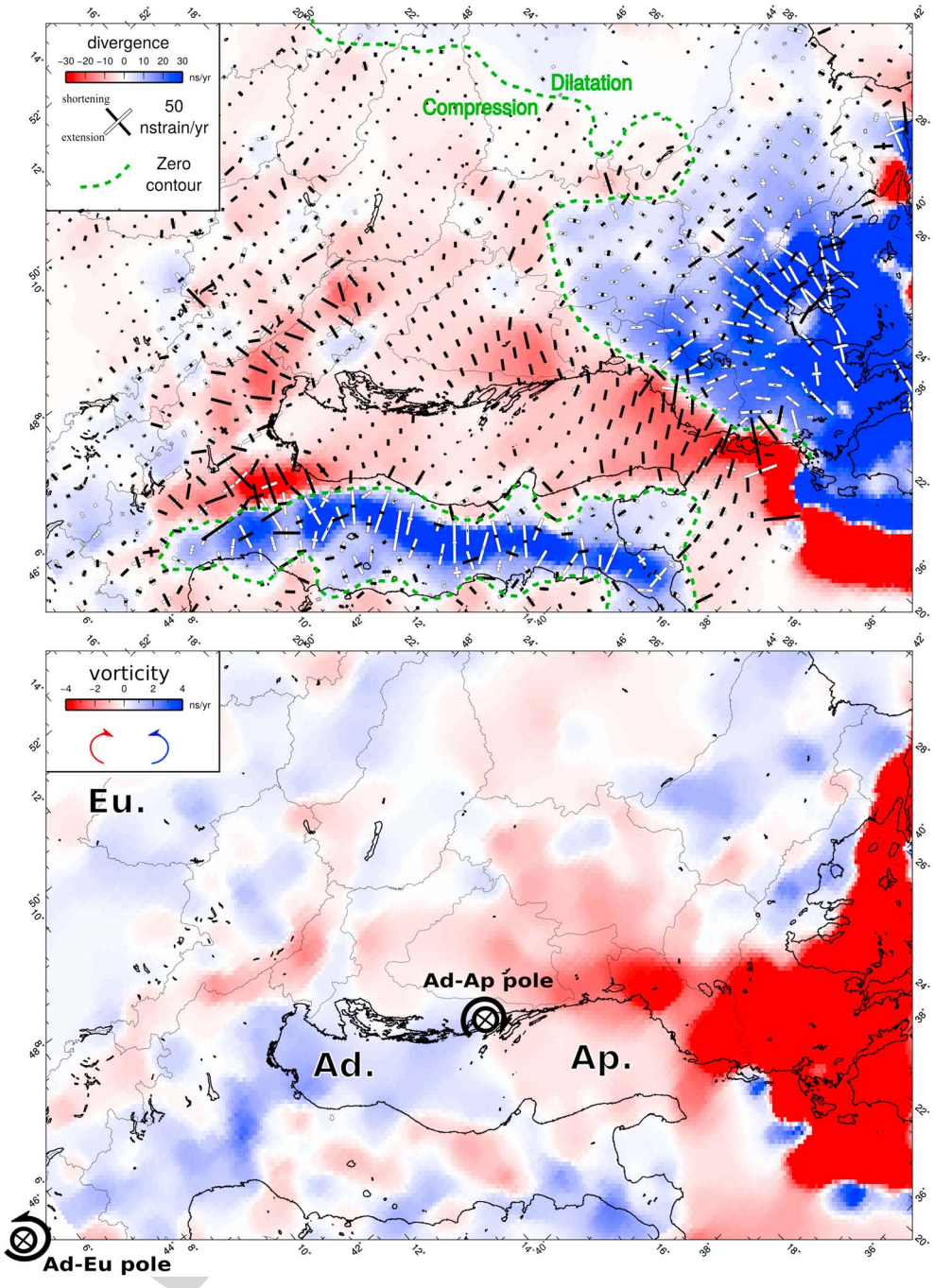

Figure 7. (a) Map of the first invariant of the strain rate tensor (or divergence) and principal strain directions. Positive values: dilatation; negative: compression. Dashed green curve: zero-divergence contour. (b) Magnitude of the vorticity of the interpolated velocity field shown in Figure 5.

studies [*D'Agostino et al.*, 2008; *Cheloni et al.*, 2014]. The Adria-Apulia Euler pole (43.02°N, 16.60°E, 0.422°/Myr) is located on the eastern Adriatic coast, in front of the diffuse boundary between the two blocks, where relatively high seismicity rates are observed offshore Adriatic Sea (Figures 6 and 7b). Furthermore, as previously underlined in section 3.1, very little compression is required in Croatia. Even if we lack dense measurements there, it seems that the western part of Croatia and the Istria Peninsula is moving together with the Adria microplate. High strain rates ($\sim 25 \times 10^{-9}$/yr) are observed across the Eastern Alps thrust front and the peri-Adriatic fault.

The calculated dilatation rate and principal strain components give new insights into the regional style of deformation (Figure 7a). As expected, dilatation is dominant in the Apennines and the Aegean Sea, while compression is occurring all along the Hellenic subduction backstop, along the northern flank of the Apennines [*Bennett et al.*, 2012] and across the active Eastern Alpine front [*Cheloni et al.*, 2014]. On the Balkan Peninsula, the transition from the Dinarides compression area to the South Bulgaria, Northern Greece, and Macedonia dilatation zones appears clearly: the zero-dilatation contour splits Albania into two, consistently with the change in tectonic style observed there [e.g., *Copley et al.*, 2009] and extends up to 44.5°N with a ~N-S orientation. There, it rotates toward a more E-W direction and roughly follows the orientation of the Balkan mountain belt (Figure 4). We observe a rotation of the principal dilatation strain axis from a ~N120°E orientation in the Albanian mountains to a nearly N-S orientation in Macedonia and southwestern Bulgaria and a ~N10°E direction in Central Bulgaria (Figure 7a).

4. Insights on Lithosphere Dynamics From the Strain Rate Field

The deformation of the continental lithosphere could be driven by several forces [e.g., *Thatcher*, 2009]: kinematic conditions applied to major plate boundaries, dragging effects from underneath the lithosphere due to convective motions of the astenospheric mantle [*Faccenna et al.*, 2013; *Le Pichon and Kreemer*, 2010], body forces generated by rheological variations within the lithosphere, and horizontal gradients of gravitational potential energy (GPE). The latter contribution can be quantified within the framework of the "thin viscous sheet" approach (TVS) [*England and McKenzie*, 1982] or using the "density moment" law [*Fleitout and Froidevaux*, 1982], and its physical formulation provides a relationship between spatial gradients of vertically averaged deviatoric stresses and GPE. In the following, we use the estimated strain rate field obtained from observed GPS velocities to assess the role of gravitational forces in driving the deformation of the lithosphere following the approach described by *England and Molnar* [1997].

4.1. Testing the Fluid Lithosphere Hypothesis

Assuming that spatial gradients of GPE are the main factors driving surface deformation, we consider the lithosphere as a continuous medium that deforms as a fluid submitted to gravitational forces only. Neglecting inertial terms, the stress balance (or Stokes) equation for a steady state fluid-like lithosphere is

$$\frac{\partial \sigma_{ij}}{\partial x_j} = -\rho g_i \tag{1}$$

where σ_{ij} is the ijth component of the stress tensor, x_j is the jth direction, ρ is the density, and g_i is the ith component of gravity acceleration [*Malvern*, 1969]. Considering that shear tractions are negligible at the bottom and top of the lithosphere and that isostasy applies, equation (1) can be written as

$$\partial_x \bar{\tau_{xx}} + \partial_y \bar{\tau_{xy}} - \partial_x \bar{\tau_{zz}} = \frac{\partial_x \Gamma}{L} \tag{2}$$

$$\partial_y \bar{\tau_{yy}} + \partial_x \bar{\tau_{xy}} - \partial_y \bar{\tau_{zz}} = \frac{\partial_y \Gamma}{L} \tag{3}$$

where $\bar{\tau_{ij}}$ is the ijth component of the deviatoric stress tensor averaged on the entire column of lithosphere [*England and Jackson*, 1989]. Γ is the gravitational potential energy (GPE) defined as

$$\Gamma = -\int_0^L \sigma_{zz}(z)\mathrm{d}z = g\int_0^L \int_0^z \rho(z')\mathrm{d}z'\mathrm{d}z \tag{4}$$

where L is the thickness of the lithosphere (supposed constant), $\rho(z)$ is density, and $\sigma_{zz}(z)$ is the vertical component of the stress tensor σ_{ij}.

If we have a complete knowledge of the spatial distribution of the vertically averaged deviatoric stress tensor $\bar{\tau_{ij}}$, we can estimate spatial gradients of gravitational potential energy Γ from the left-hand side of equations (2) and (3). We choose to describe the rheology of the lithosphere with a "power law" defined by *Sonder and England* [1986] as

$$\tau_{ij} = 1/2B\dot{E}^{\frac{1}{n}-1}\dot{\epsilon}_{ij} \tag{5}$$

in which $\dot{E}$ is the second invariant of the strain rate tensor defined in section 3.2, and $1/2B\dot{E}^{\frac{1}{n}-1}$ is the effective viscosity of the lithosphere. Knowing $\dot{\epsilon}_{ij}$ at any grid point and assuming that B is constant over the entire area, we calculate the left member of equations (2) and (3) and integrate over the entire region to get the dimensionless GPE, denoted by Γ^* or GPE* as defined by *England and Molnar* [1997] as

$$\Gamma^* = \Gamma/BL \times (1\mathrm{s})^{1/n} \tag{6}$$

On the other hand, to independently calculate the right member of equations (2) and (3), we must calculate Γ from equation (4), which would require the unknown lithospheric density structure. Fortunately, a proxy for Γ can be obtained from topography if its supporting mechanism is specified. Here we assume that the Airy crustal isostasy controls topography through lateral crustal thickness variations, rather than the mantle-supported mechanism suggested for the Apennines [*D'Agostino et al.*, 1999, 2001]. In both cases, however, we get a relatively simple relationship between Γ and h (see also *D'Agostino et al.* [2014], for a discussion on alternative mechanisms of support). In the case of Airy isostasy, considering a column of lithosphere composed of a mantle of density ρ_m under a crust of density ρ_c and altitude h, we can use the following relation [*England and Houseman*, 1989]:

$$\Gamma = g\rho_c h\left(S_0 + \frac{\rho_m}{\rho_m + \rho_c}\frac{h}{2}\right) \tag{7}$$

where S_0 is the crustal thickness for a column of lithosphere whose surface height is zero. Following *D'Agostino et al.* [2014], we take a L =100 km thick column of lithosphere in which the crustal thickness S_0 is 30 km as a reference for the GPE calculation. We can therefore derive the GPE relative to the reference column of lithosphere directly from the ETOPO1 filtered topography (we used a 100 km width Gaussian filter), assuming ρ_c is 2800 kg.m^3 and ρ_m is 3300 kg.m^3 over the entire region (Figure 9). In order to test whether isostatic compensation is achieved in our study area, we calculate the theoretical depth of the Moho from topography assuming Airy isostasy and compare it to the Moho depth estimated from seismic wave velocities in the EPcrust model for Europe (see Figure S10 and *Molinari and Morelli*, 2011). Discrepancies between both Moho depths are not more than 5 km, in general, except in the Po Plain, the Pannonian Basin, and Macedonia where up to 20 km discrepancies are observed. Therefore, we are confident that, over the largest part of our study area (in particular in Central Apeninnes, Albanides, Dinarides, and Eastern Alps), Airy isostasy is a reasonable first-order assumption and that application of equation (7) is warranted (see section 4.3 for further discussion).

If the TVS hypothesis is valid and the lithosphere effectively behaves as a homogeneous fluid forced by gravity, equations (2), (3), and (6) apply, and there must be a linear relationship between the strain-derived GPE* and the topography-derived GPE. In Figure 8, we plot the numerically calculated GPE* contours together with the GPE* gradients $\partial_x\Gamma^*$ and $\partial_y\Gamma^*$ and the filtered ETOPO1 topography. Where equation (2) is verified, the gradients of GPE* should be similar to the gradients of topography. In other words, they should be pointing toward the highlands, following the belt orientation [e.g., *England and Molnar*, 1997]. This is clearly the case along the Central and Southern Apennines mountain belt, where the highest values of GPE* are observed along the regional topographic culmination (the correlation coefficient r between GPE* and GPE calculated from topography is 0.71, see Figure 9). This result supports the earlier analyses from *D'Agostino et al.* [2014] obtained from 2-D sections across the Apennines and strengthens their conclusion. F8 F9

An even clearer correlation (r = 0.89) between GPE* and the GPE derived from the topography is observed over the Albanides (Figures 8 and 9). This result argues for a dominant control of gravity on the current-day deformation of Albania as previously suggested by *Copley et al.* [2009].

On the contrary, no correlation is observed between the strain-derived GPE* and the topography in the Eastern Alps and the Dinarides. In these regions, we observe a decrease of the GPE* in the vicinity of the active fronts (the Eastern Alps thrust and the offshore western Dinarides thrust, respectively) followed by an increase of the GPE* away from this fault line. This pattern is roughly consistent with the one predicted by elastic deformation theory on active thrusts (Figure S11). Therefore, the deformation occurring in these regions is at least partly governed by elastic loading on what could be considered as Adria-Apulia rigid blocks boundaries.

In the Northern Apennines where the correlation between GPE* and topography is relatively low, our assumption of Airy isostasy is debatable (see Figure S10 and section 4.3 for further discussion) and elastic loading effect on the Ferrara thrust could drive part of the deformation. The situation is less clear in the eastern Balkans,

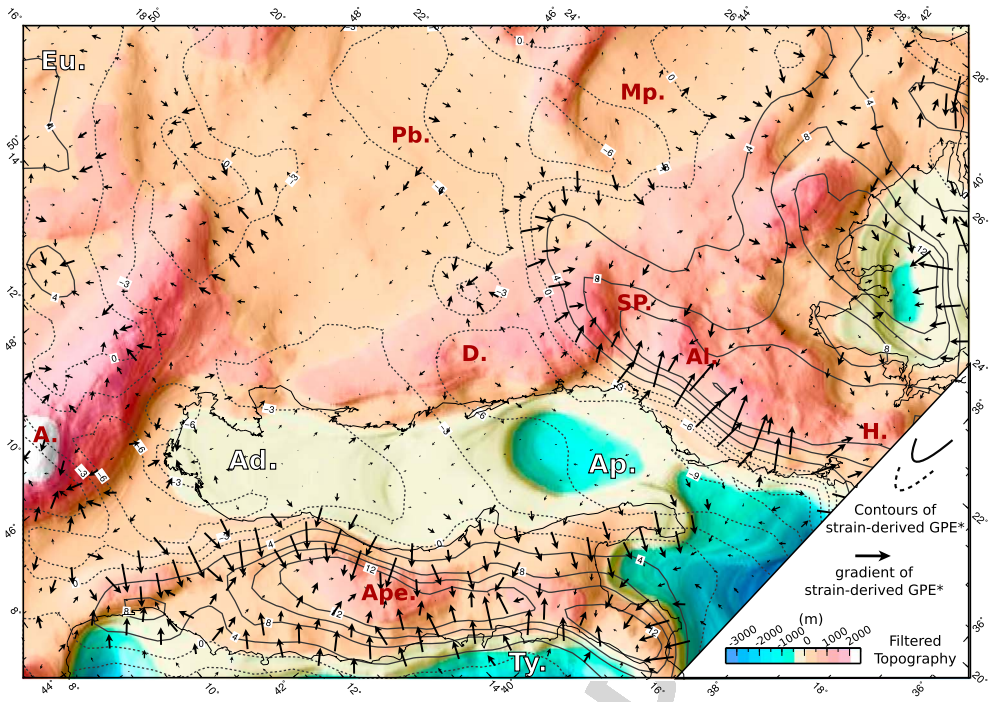

Figure 8. Strain-derived gravitational potential energy. Arrows show gradients of dimensionless gravitational potential energy (GPE*), derived by assuming a power law rheology for the lithosphere with $n = 3$ (see equation (5)). Values of GPE* integrated from GPE gradients and multiplied by a factor of 10^6 are contoured and plotted together with the filtered topography from ETOPO1. Same labels as in Figures 1 and 5.

in Macedonia, and across the Balkan mountain belt where GPE gradients seem to have a minor influence on the surface deformation pattern (Figure 8). The Eurasia-Anatolia plate boundary along the North Anatolian Fault is a zone of localized weakness, and our analysis of the lithosphere as a continuous medium is not applicable.

4.2. Lithosphere Effective Viscosity Estimates

We now consider the two mountain belts in which the correlation between the dimensionless GPE* and the GPE calculated from topography is significant ($r > 0.5$), i.e., the Apennines and Albanides (Figure 9). The slope of the linear correlation obtained in Figure 9 gives us an estimate of $BL \times (1\ \mathrm{s})^{1/n}$ for each region (equation (6)) and therefore allows us to calculate the lithosphere effective viscosity for a given strain rate and a value of the exponent n. Assuming $L \sim 100$ km and $n = 3$ as derived from laboratory studies [e.g., *Sonder and England*, 1986], we find viscosity values between 2×10^{21} and 5×10^{21} Pa s for the Albanides and Apennines lithospheres (Table 1), i.e., similar to the effective viscosities found by *D'Agostino et al.* [2014] and other studies in distinct mountain belts [e.g., *England and Molnar*, 1997; *Vergnolle et al.*, 2007]. Assuming a Newtonian rheology, i.e., $n = 1$, gives values for the lithosphere viscosity η between 3.0×10^{21} Pa s and 3.4×10^{21} Pa s (see additional supporting information and Figure S12).

4.3. Main Limitations

By testing the fluid lithosphere hypothesis using the method presented in section 4.1, we aim at testing how far we can go in the understanding of the lithosphere dynamics using very simple assumptions. On the other hand, several limitations can affect our test [e.g., *England and Molnar*, 1997]: (i) we consider no lateral change in rheological properties of the lithosphere over the entire region, therefore considering that B is constant in equation (5); (ii) we assume crustal Airy isostasy as the compensation mechanism over the entire region; and (iii) basal shear traction is supposed to be negligible in equations (2) and (3).

This latter assumption is probably reasonable in our study area except for regions where significant basal traction may arise from lithospheric scale thrusts like the Eastern Alps front, the Dinarides, and the Northern Apennines under which a dipping slab has been detected [*Bennett et al.*, 2008]. As previously discussed and shown in Figure S10, the Airy isostasy is not achieved everywhere in particular in the large sedimentary basins

this figure doest not have to be the largest of the entire paper. It could be reduced.

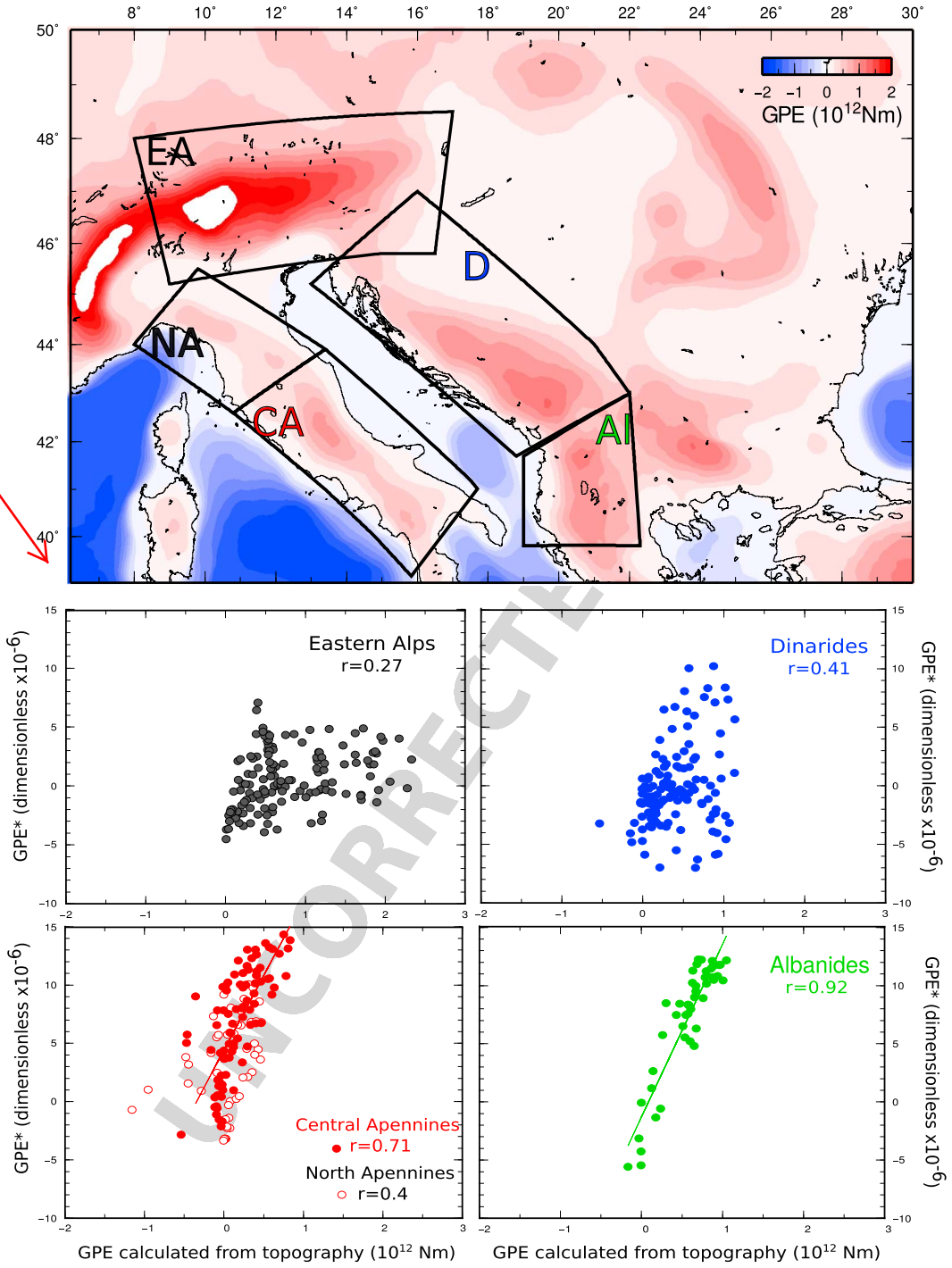

Figure 9. Testing topography control on the peri-Adriatic belts deformation. (top) Map of the GPE calculated from filtered ETOPO1 topography (see equation (7)) assessing Airy isostasy. (bottom) Calculated GPE* from strain, as contoured in Figure 8 against the GPE calculated from topography for several subregions as contoured on the upper map. Least square-estimated best fit linear regressions are plotted as colored lines for Central Appennines and Albanides where the correlation is significant, i.e., where the correlation coefficient *r* is higher than 0.5.

Table 1. Effective Viscosity Calculated for the Central Apennines and the Albanides Mountain Belts for $n=3$ or $n=1$ (Newtonian Rheology)[a]

Area	B (N m^{-2} s$^{1/n}$)	$\dot{E}$ (nstrain/yr)	Effective Viscosity (Pa s)	η (Pa s)
Central Apennines	5.8×10^{11}	~50	2.1×10^{21}	3×10^{21}
Albanides	5.3×10^{11}	~30	5.4×10^{21}	3.4×10^{21}

[a]In case $n=3$, B is derived from the slope between the dimensionless GPE* and the GPE calculated from topography, taking $L=100$ km. $\dot{E}$ is averaged for both areas from the calculated strain rate tensor.

like the Po Plain and the Pannonian Basin. More generally, ignoring spatial variations in the thermal structure of the lithosphere can significantly bias our local estimate of GPE [e.g., *,Fleitout and Froidevaux*, 1982; *Copley*, 2008].

Finally, considering a constant B parameter for such a large and complex region is not realistic: one can expect important lateral variations in the lithosphere's effective viscosity across the Alps for instance [e.g., *Willingshofer and Cloetingh*, 2003; *Robl and Stüwe*, 2005] or near the Aegean domain. Considering a simpler 2-D problem as suggested by *England and Molnar* [1997], an unaccounted lateral variation ΔB would propagate into the calculated GPE as an error $\Delta\Gamma$ given by

$$\Delta\Gamma = L\dot{\epsilon}_{xx}^{1/n} \times \Delta B \tag{8}$$

Therefore, in our study, variations of B could ~~therefore~~ bias our simple GPE estimates by 10^{11} to 10^{12} N m ($L=100$ km, $n=3$, and $\dot{\epsilon}_{xx}$ ~30 nstrain/yr). Investigating such lateral variations in the lithosphere's rheology is beyond the scope of this study but will be required for a deeper understanding of the regional dynamics.

5. Discussion

5.1. Kinematic and Dynamics of the Balkan Peninsula

5.1.1. Rotations in the Balkans

The velocity field presented in this work shows that the western Balkans Peninsula, including the Albanides and the Northern Hellenides, is experiencing a clockwise rotation around Northern Albania, approximately in the Scutari-Peck transform zone (Figures 4 and 5). This is significantly different from what was found in previous studies in which the northern end of this rotation cell was not resolved [e.g., *Perouse et al.*, 2012; *Reilinger et al.*, 2010; *Nyst and Thatcher*, 2004]. However, in agreement with these studies, we confirm that the southern edge of the rotating region is located near the boundary between Albania and Greece, i.e., more than 150 km south of the Scutari-Peck area.

According to paleomagnetic studies, the Scutari-Peck zone is also known to be a boundary between two paleomagnetic domains, the Dinarides, and the Albanides, the latter rotating clockwise since the early Miocene at least [*Kissel et al.*, 1985; *Speranza et al.*, 1995; *Kissel et al.*, 1995; *Van Hinsbergen et al.*, 2005], while no clear rotation has been detected in the Dinarides domain [e.g., *Márton and Veljovic*, 1983]. *Kissel et al.* [1995]'s paleomagnetic measurements argue for a ~45° clockwise rotation of the Albanides since the lower Miocene (from 23 to 16 Myr), equivalent to a rotation rate of ~2°/Myr. These authors interpreted the observed decrease in the rotation amplitude in the vicinity of the Scutari-Peck region as an argument in favor of a semirigid rotation of the entire Albanides region around a Euler pole located in the Scutari-Peck area (19.75°E, 41.5°N). Such a rotation would overpredict by several millimeter per year our interpolated velocity field in the Dinarides and Northern Greece (Figure S8). However, it predicts E-W oriented horizontal velocities lower than 5 mm/yr in Central Albania, i.e., of roughly the magnitude and direction of the current-day measurements (Figure S8). Finally, we conclude that even if the current rotation observed from our GPS velocity field is not well described by a rigid Eulerian rotation on a sphere, our results suggest that the post-Eocene clockwise rotation of the Albanides and Northern Greece around the Scutari-Peck region is occurring today at rates not significantly different from the paleomagnetic estimates, given their uncertainty [*Demarest*, 1983].

5.1.2. Dynamics of the Dinarides-Albanides System

According to *Picha* [2002], the transition from a purely compressive deformation affecting both the Dinarides and Albanides regions to the current southwestward oriented motion of the inner Balkans (Serbia and Macedonia) occurred when the thickening of the crust in the Pannonian Basin impeded further propagation

of the mountain front to the North East, i.e., in the last stage of the Dinarides mountain building. This hypothesis implies that a relatively free southern boundary drives the lithosphere southward toward the Aegean domain.

The retreat of the Nubian lithospheric slab involved in the Hellenic subduction [e.g., *Jolivet et al.*, 2013] is a good candidate for driving the Balkan lithosphere flux toward the extending Aegean Sea. Indeed, several authors have shown that mantle anisotropy in the entire Aegean domain was mainly directed NE-SW, i.e., perpendicular to the Hellenic trench [e.g., *Paul et al.*, 2014; *Olive et al.*, 2014], in agreement with a large mantle flux driven by slab suction [*Faccenna et al.*, 2013]. Therefore, it is probable that the southward flow observed at the surface in the southern Balkans (south of 44.5°N, Figure 6) results from the same suction effect. Alternatively, large-scale rotation patterns observed at the surface in Northern Greece and Anatolia have been proposed to result from asthenospheric toroidal flows developing on the western and eastern edges of the Hellenic subduction zone, respectively, due to slab tearing [e.g., *Perouse et al.*, 2012; *Suckale et al.*, 2009; *Royden and Papanikolaou*, 2011; *Le Pichon and Kreemer*, 2010].

Whatever the cause, the deep mantle motions that may occur under the peri-Adriatic area remain poorly understood. The sparse shear wave splitting (SKS) measurements available in Serbia, Albania, and Hungary (i.e., under our study area) show a NW-SE orientation [*Wüstefeld et al.*, 2009] (Figure S9), but they are too few and too poorly constrained in depth to infer any possible correlation between deep mantle motion and surface displacements. Recent anisotropic seismic velocity models based on surface wave dispersion may provide more precise depth resolution of the mantle anisotropy and could help in the future to investigate this correlation [e.g., *Debayle and Ricard*, 2013]. Overall, as underlined by *Paul et al.* [2014] for Anatolia, the surface deformation pattern is often much more complex than the relatively homogeneous anisotropy directions reflecting the mantle motion. This speaks in favor of contributions of other driving mechanisms for the current-day surface motion than the mantle drag effect alone.

While several tomographic studies have shown that continental collision is going on under the southern Hellenides (north of the Kephalonia fault [e.g., *Royden and Papanikolaou*, 2011; *Olive et al.*, 2014]) and the central Dinarides [*Bennett et al.*, 2008], it is still unclear if a slab is present under Albania [*Piromallo and Morelli*, 2003]. In any case, these slowly converging collision zones may not be able to generate large-scale mantle flows that could drive surface deformation. The current deformation observed across the Dinarides appears to be mainly due to interseismic elastic loading on the main frontal thrust of this collisional system, while the important GPE gradients between the external Dinarides and the Pannonian Basin have no or little influence on it [*Bennett et al.*, 2008] (Figure 8). This active thrust accommodates a large part of the Adria-Apulia push and the strength of its interface appears large enough to support the Dinarides topography.

In contrast, the simple test based on the momentum balance equation (section 4) is verified in the Albanides, suggesting the important role of horizontal gradients of gravitational potential energy in controlling the deformation. In other words, gradients of strain rates are correlated with gradients of GPE, implying that the current pattern of deformation observed in the Albanides may be to the first order driven by the elevation contrasts between the mountain belt and the western lowlands. Therefore, GPS measurements, despite being sparse in the area, support the finding of *Copley et al.* [2009] that argue for a gravity-driven change in tectonic styles between eastern Albania (where the focal mechanisms show mainly extension) and western Albania (where the focal mechanisms show compression and strike-slip motion). These authors propose that the large thickness of sediments deposited in western Albania during Mezosoic and Cenozoic time could have heated and sufficiently weakened the lithosphere so that it is unable to sustain the large GPE gradients generated during the preceding mountain building phase. It may be notable that large amounts of salt and evaporites outcrop in the Albanian lowlands, often forming diapirs or decollement layers associated with large thrusts [e.g., *Velaj*, 2001]. These weak layers could have lowered the stress on the eastern Albania thrusts system, thus favoring a gravity-controlled deformation of the Albanides. The strong obliquity between the Apulia-Nubia northeastward push and the Albanides, or the presence of a more buoyant portion of the Apulia lithosphere in front of Albania, could also generate the low stress required on the western front of the Albanides.

Thus, besides being the result of the same regional collisional environment, the Dinarides and Albanides mountain belts are currently deforming following completely different processes. While the Dinarides are still sustained by an active front located at the boundary with the Adriatic crust, the Albanides are extending mainly due to large gravitational potential energy gradients that cannot be supported by the thrusts system to the west.

Therefore, we propose that the overall rotation observed in the western Balkans results from (i) the active compression still going on across the Dinarides, (ii) the Hellenic slab suction effect generating an extensional domain up to Central Serbia, and (iii) the stress decrease on the western Albanian mountain front leading to a gravity-driven collapse of this ~~mountain~~ belt toward the Adriatic.

5.2. Dynamics of the Apennines

Several models have been proposed to explain the topography and current deformation of the 500 km long Apennines belt. This deformation is dominated by extension localized at the highest point of the belt in the Central and Southern Apennines, while compression is confined across the Ferrara thrust front in the Northern Apennines [e.g., *D'Agostino et al.*, 2008; *Serpelloni et al.*, 2005]. Based on tomographic images showing a deep high V_p and V_s anomaly under the North Apennines belt [e.g., *Benoit et al.*, 2011], several authors propose that slab retreat, delamination, or slab tearing could be the main factors controlling surface deformation [e.g., *Bennett et al.*, 2012]. Slab suction forces have also been proposed as support mechanisms for topography in the Central and Southern Apennines [e.g., *Cavinato and De Celles*, 1999; *Devoti et al.*, 2011] since SKS fast axis direction are consistent with trench rollback [*Margheriti et al.*, 2003] (and Figure S9). It has also been suggested that Apennine topography could be supported by mantle convection [*D'Agostino et al.*, 1999, 2011].

The correlation observed between the topography gradients and the strain gradients is less significant in the northern Apennines (Figures 8 and 9). There, a combination of elastic loading on the Adria-Apennines boundary, mantle drag, and GPE gradients is probably driving the surface deformation.

~~However,~~ in a recent study focused on the Central Apennines, *D'Agostino et al.* [2014] show that the observed deformation pattern is probably driven by differences in GPE due to lateral elevation contrasts in an overall diverging context, in disagreement with arguments that slab suction alone could drive the surface deformation. Our results support the hypothesis of a GPE-driven deformation all over the south-central Apennines (see section 4 and Figures 8 and 9), suggesting that slab suction is playing a minor role in the current deformation of the belt. In contrast with major mountain belts like the Andes and the Himalaya where extension is observed only at very high elevations because of high stresses applied on their main active front, the extensional boundary conditions along most of the Apennines due to Tyrrhenian and Adria-Apulia divergent motions allow GPE gradients to drive deformation at low elevation.

5.3. Dynamics of the Eastern Alps

The most obvious feature of the deformation field in the Eastern Alps (Figure 3) is a clockwise rotation of Slovenia (Figure 7b) and an overall eastward motion. The eastward motion of the central part of the belt has been previously described from geodesy, geology, and background seismicity and has often been interpreted as an escape of the inner part of the belt between two major strike-slip structures (the peri-Adriatic fault to the south and the Salzach-Ennstal fault to the north) in response to the Adria indenter push [e.g., *Ratschbacher et al.*, 1991]. The motion of the Adria region is partly accommodated on the southeastern Alps thrust front that has been recently proven to be mainly interseismically locked [*Cheloni et al.*, 2014]. This is consistent with the large northward decrease observed in Figures 3 and 5b in horizontal velocities across the front. However, several models propose that gravitational collapse of the belt toward the Pannonian Basin (equivalent to GPE-driven deformation) occurs together with partial extrusion of the Eastern Alps [*Selverstone*, 2004, and references therein]. Some attempts have been made to quantify the relative influence of both mechanisms on the deformation [e.g., *Robl and Stüwe*, 2005], but the lack of dense GPS measurements prevented from comparing model predictions and observations.

Our new velocity field shows that, in contrast with what would be expected for extrusion, the eastward motion toward the Pannonian Basin is not restricted to the mountain belt itself. Indeed, even the Alpine forelands and the Bohemian Massif appear to share an eastward residual motion relative to stable Eurasia. We observe a significant change in the azimuth of the horizontal velocities from one side of the Peri-Adriatic fault to the other (Figure 3) suggesting that part of the Adria push motion is accommodated there, but no change of velocity is observed across the Salzach-Ennstal fault nor across the northernmost topographic front of the belt, in disagreement with some previously published velocity fields [*Caporali et al.*, 2009]. Furthermore, we showed in section 4 that GPE gradients are probably not the dominant force driving the deformation of the Eastern Alps; i.e., there is no significant correlation between the gradients of strain and the gradients of topography. Thus, the current-day velocity field presented in this study indicates that neither extrusion nor GPE gradients alone could drive the regional eastward motion.

The hypothesis of a constant lithosphere rheology over such a broad region encompassing very different lithospheric structures [*Molinari and Morelli*, 2011] such as the Eastern Alps (where the crust and lithosphere has been significantly thickened) and the Pannonian Basin (in which the crust have been thinned and overlaid by large thickness of sediments) is probably not correct (see section 4.3). More complex models including some of the detected rheological contrasts across the belt [e.g., *Brückl et al.*, 2010; *Bianchi et al.*, 2014], its foreland, and the Adria indenter are required to evaluate the role of strength heterogeneity [e.g., *Robl and Stüwe*, 2005; *Copley*, 2008]. Furthermore, seismic and gravimetric studies conducted across the Eastern Alps show that a cold lithospheric root exists beneath the belt [*Bianchi et al.*, 2014; *Ebbing et al.*, 2006]. Such a deep density anomaly could cancel the effect of the shallower light crustal root and would trigger compression rather than extension on the crest of the belt [*Fleitout and Froidevaux*, 1982]. Using more complex lithospheric structure models to calculate the gravitational potential energy might well change our results for this mountain belt.

Finally, one cannot rule out that the eastward regional motion is caused by a deep and large-scale motion of the mantle. However, to our knowledge, this kind of deep motion has not been observed that far. Therefore, further modeling efforts are required to better understand the dynamics of the Eastern Alps.

6. Conclusion

We obtained a new GPS velocity field particularly dense in the inner Balkans, Slovenia, and Eastern Alps that we have carefully tied to the stable Eurasian plate by the use of a new reference frame realization. The current deformation field derived from these measurements shows a sharp clockwise rotation of the western Balkans around North Albania in the Scutari-Peck region together with a broad eastward motion of the Eastern Alps and associated forelands toward the Pannonian Basin. Together with dense measurements along the Italian Peninsula, they form a nearly continuous picture of the deformation over the peri-Adriatic region that we use to calculate the strain rate distribution.

We take advantage of this strain rate field derived from GPS measurements to test whether the observed deformation across the various continental collision belts could be the result of a viscous lithosphere deforming due to horizontal gradients of gravitational potential energy (GPE). It appears that in the case of the Central Apennines and of the Albanides the current deformation is most likely driven by GPE gradients applied on a viscous lithosphere ($\eta \sim 3 \times 10^{21}$ Pa s), while mantle drag or rheological heterogeneities do not significantly affect the deformation pattern. In contrast, the deformation observed in the Dinarides and Eastern Alps belts may result from elastic loading on frontal thrusts, mantle-driven motion, or complex lithospheric rheology contrasts that we did not take into account in this study.

Therefore, since the stress on the frontal thrusts of the belts must be low for GPE to drive deformation, the western thrusts of the Albanides are probably supporting lower stresses than the western Dinarides thrust system, allowing the Albanian lithosphere to flow. In Albania, since the regional clockwise rotation pattern is in good agreement with paleomagnetic measurements, it appears that the current rotation of the Albanides around the Scutari-Peck transverse zone is continuing at rates that have been unchanged since the Miocene.

The simple method proposed here to quantify the role of gravitational potential energy on the dynamics of a slowly deforming region should be refined in the future to account for lateral variations of lithosphere rheology and kinematic boundary conditions.

Acknowledgments
This work has been funded by the AXA Research Fund Postdoctoral Program. We are grateful to the institutions and networks in the Balkans for freely sharing the data, namely, AGROS, APOS, NOA, MAKPOS, METRICA, SIGNAL, TGREF, HEMUSNET, and other networks listed in the supporting information. The velocities obtained from our calculation are provided in the supporting information. We thank J.Haines, W.Holt, and C.Kreemer for making the Sparse code available, and A.Copley, G.Selvaggi, and P.England for their fruitful discussions. We are also grateful to W.Thatcher for the constructive and thorough review.

References

Altamimi, Z., X. Collilieux, and L. Métivier (2011), ITRF2008: An improved solution of the international terrestrial reference frame, *J. Geod.*, *85*(8), 457–473.

Ambraseys, N., and J. Jackson (1998), Faulting associated with historical and recent earthquakes in the Eastern Mediterranean region, *Geophys. J. Int.*, *133*(2), 390–406.

Bar-Sever, Y. E., P. M. Kroger, and J. A. Borjesson (1998), Estimating horizontal gradients of tropospheric path delay with a single GPS receiver, *J. Geophys. Res.*, *103*(B3), 5019–5035.

Beavan, J., and J. Haines (2001), Contemporary horizontal velocity and strain rate fields of the Pacific-Australian plate boundary zone through New Zealand, *J. Geophys. Res.*, *106*(B1), 741–770, doi:10.1029/2000JB900302.

Bennett, R., et al. (2012), Syn-convergent extension observed using the retreat GPS network, Northern Apennines, Italy, *J. Geophys. Res.*, *117*, B04408, doi:10.1029/2011JB008744.

Bennett, R. A., S. Hreinsdóttir, G. Buble, T. Bašić, Ž. Bačić, M. Marjanović, G. Casale, A. Gendaszek, and D. Cowan (2008), Eocene to present subduction of Southern Adria mantle lithosphere beneath the dinarides, *Geology*, *36*(1), 3–6.

Benoit, M. H., M. Torpey, K. Liszewski, V. Levin, and J. Park (2011), *P* and *S* wave upper mantle seismic velocity structure beneath the northern Apennines: New evidence for the end of subduction, *Geochem. Geophys. Geosyst.*, *12*, Q06004, doi:10.1029/2010GC003428.

Bertiger, W., S. D. Desai, B. Haines, N. Harvey, A. W. Moore, S. Owen, and J. P. Weiss (2010), Single receiver phase ambiguity resolution with GPS data, *J. Geod.*, *84*(5), 327–337.
Bianchi, I., M. S. Miller, and G. Bokelmann (2014), Insights on the upper mantle beneath the Eastern Alps, *Earth Planet. Sci. Lett.*, *403*, 199–209.
Blewitt, G. (1998), GPS data processing methodology: From theory to applications, in *GPS for Geodesy*, edited by P. Teunissen and A. Kleusberg, pp. 231–270, Springer, Berlin Heidelberg.
Blewitt, G., C. Kreemer, W. C. Hammond, and J. M. Goldfarb (2013), Terrestrial reference frame NA12 for crustal deformation studies in North America, *J. Geodyn.*, *72*, 11–24.
Böhm, J., A. Niell, P. Tregoning, and H. Schuh (2006), Global Mapping Function (GMF): A new empirical mapping function based on numerical weather model data, *Geophysical Research Letters*, *33*, L07304, doi:10.1029/2005GL025546.
Brückl, E., M. Behm, K. Decker, M. Grad, A. Guterch, G. Keller, and H. Thybo (2010), Crustal structure and active tectonics in the Eastern Alps, *Tectonics*, *29*, TC2011, doi:10.1029/2009TC002491.
Brun, J.-P., and D. Sokoutis (2010), 45 m.y. of Aegean crust and mantle flow driven by trench retreat, *Geology*, *38*(9), 815–818.
Burchfiel, C., R. W. King, A. Todosov, V. Kotzev, N. Durmurdzanov, T. Serafimovski, and B. Nurce (2006), GPS results for Macedonia and its importance for the tectonics of the Southern Balkan extensional regime, *Tectonophysics*, *413*(3), 239–248.
Caporali, A., et al. (2009), Surface kinematics in the Alpine-Carpathian-Dinaric and Balkan region inferred from a new multi-network GPS combination solution, *Tectonophysics*, *474*(1), 295–321.
Cavinato, G., and P. De Celles (1999), Extensional basins in the tectonically bimodal Central Apennines fold-thrust belt, Italy: Response to corner flow above a subducting slab in retrograde motion, *Geology*, *27*(10), 955–958.
Cheloni, D., N. D'Agostino, and G. Selvaggi (2014), Interseismic coupling, seismic potential, and earthquake recurrence on the southern front of the Eastern Alps (NE Italy), *J. Geophys. Res. Solid Earth*, *119*, 4448–4468, doi:10.1002/2014JB010954.
Chen, Q., J. T. Freymueller, Q. Wang, Z. Yang, C. Xu, and J. Liu (2004), A deforming block model for the present-day tectonics of Tibet, *J. Geophys. Res.*, *109*, B01403, doi:10.1029/2002JB002151.
Copley, A. (2008), Kinematics and dynamics of the southeastern margin of the Tibetan Plateau, *Geophys. J. Int.*, *174*(3), 1081–1100.
Copley, A., F. Boait, J. Hollingsworth, J. Jackson, and D. McKenzie (2009), Subparallel thrust and normal faulting in Albania and the roles of gravitational potential energy and rheology contrasts in mountain belts, *J. Geophys. Res.*, *114*, B05407, doi:10.1029/2008JB005931.
D'Agostino, N., et al. (1999), Convective support of long-wavelength topography in the Apennines (Italy), *Terra Nova*, *11*(5), 228–233.
D'Agostino, N., J. Jackson, F. Dramis, and R. Funiciello (2001), Interactions between mantle upwelling, drainage evolution and active normal faulting: An example from the Central Apennines (Italy), *Geophys. J. Int.*, *147*(2), 475–497.
D'Agostino, N., A. Avallone, D. Cheloni, E. D'anastasio, S. Mantenuto, and G. Selvaggi (2008), Active tectonics of the Adriatic region from GPS and earthquake slip vectors, *J. Geophys. Res.*, *113*, B12413, doi:10.1029/2008JB005860.
D'Agostino, N., S. Mantenuto, E. D'Anastasio, R. Giuliani, M. Mattone, S. Calcaterra, P. Gambino, and L. Bonci (2011), Evidence for localized active extension in the central Apennines (Italy) from global positioning system observations, *Geology*, *39*(4), 291–294.
D'Agostino, N., P. England, I. Hunstad, and G. Selvaggi (2014), Gravitational potential energy and active deformation in the Apennines, *Earth Planet. Sci. Lett.*, *397*, 121–132.
Debayle, E., and Y. Ricard (2013), Seismic observations of large-scale deformation at the bottom of fast-moving plates, *Earth Planet. Sci. Lett.*, *376*, 165–177.
Demarest, H. H. (1983), Error analysis for the determination of tectonic rotation from paleomagnetic data, *J. Geophys. Res.*, *88*(B5), 4321–4328.
Devoti, R., A. Esposito, G. Pietrantonio, A. R. Pisani, and F. Riguzzi (2011), Evidence of large scale deformation patterns from GPS data in the Italian subduction boundary, *Earth Planet. Sci. Lett.*, *311*(3), 230–241.
Ebbing, J., C. Braitenberg, and H.-J. Götze (2006), The lithospheric density structure of the Eastern Alps, *Tectonophysics*, *414*(1), 145–155.
England, P., and G. Houseman (1989), Extension during continental convergence, with application to the Tibetan Plateau, *J. Geophys. Res.*, *94*(B12), 17,561–17,579.
England, P., and J. Jackson (1989), Active deformation of the continents, *Annu. Rev. Earth Planet. Sci.*, *17*, 197–226.
England, P., and D. McKenzie (1982), A thin viscous sheet model for continental deformation, *Geophys. J. Int.*, *70*(2), 295–321.
England, P., and P. Molnar (1997), Active deformation of Asia: From kinematics to dynamics, *Science*, *278*(5338), 647–650.
Faccenna, C., T. W. Becker, L. Jolivet, and M. Keskin (2013), Mantle convection in the Middle East: Reconciling Afar upwelling, Arabia indentation and Aegean trench rollback, *Earth Planet. Sci. Lett.*, *375*, 254–269.
Fleitout, L., and C. Froidevaux (1982), Tectonics and topography for a lithosphere containing density heterogeneities, *Tectonics*, *1*(1), 21–56.
Flesch, L. M., W. E. Holt, A. J. Haines, and B. Shen-Tu (2000), Dynamics of the Pacific-North American plate boundary in the western United States, *Science*, *287*(5454), 834–836.
Galasso, C., I. Gomez, A. Gupta, and B. Shen-Tu (2013), Probabilistic seismic hazard assessment for Albania, Macedonia and Serbia, *paper presented at Skopje Earthquake — 50 Years of European Earthquake Engineering*, Skopje, Macedonia, 29–31 May.
Haines, A., and W. Holt (1993), A procedure for obtaining the complete horizontal motions within zones of distributed deformation from the inversion of strain rate data, *J. Geophys. Res.*, *98*(B7), 12,057–12,082.
Haslinger, C., S. Krauss, and G. Stangl (2007), The intra-plate velocities of GPS permanent stations of the Eastern Alps, *Vermessung Geoinformation*, *2*, 66–72.
Hugentobler, U., R. Dach, P. Fridez, and M. Meindl (2006), Bernese GPS software, version 5.0.
Jolivet, L., et al. (2013), Aegean tectonics: Strain localisation, slab tearing and trench retreat, *Tectonophysics*, *597*, 1–33.
Jouanne, F., J. Mugnier, R. Koci, S. Bushati, K. Matev, N. Kuka, I. Shinko, S. Kociu, and L. Duni (2012), GPS constraints on current tectonics of Albania, *Tectonophysics*, *554*, 50–62.
Kissel, C., C. Laj, and C. Müller (1985), Tertiary geodynamical evolution of northwestern Greece: Paleomagnetic results, *Earth Planet. Sci. Lett.*, *72*(2), 190–204.
Kissel, C., F. Speranza, and V. Milicevic (1995), Paleomagnetism of external southern and central Dinarides and northern Albanides: Implications for the Cenozoic activity of the Scutari-Pec transverse zone, *J. Geophys. Res.*, *100*(B8), 14,999–15,007.
Le Pichon, X., and C. Kreemer (2010), The Miocene-to-present kinematic evolution of the eastern Mediterranean and Middle East and its implications for dynamics, *Annu. Rev. Earth Planet. Sci.*, *38*, 323–351.
Malvern, L. E. (1969), *Introduction to the Mechanics of a Continuous Medium*, Prentice-Hall, Univ. of Michigan.
Margheriti, L., F. Lucente, and S. Pondrelli (2003), SKS splitting measurements in the Apenninic-Tyrrhenian domain (Italy) and their relation with lithospheric subduction and mantle convection, *J. Geophys. Res.*, *108*(B4), 2218, doi:10.1029/2002JB001793.
Márton, E., and D. Veljovic (1983), Paleomagnetism of the Istria peninsula, Yugoslavia, *Tectonophysics*, *91*(1), 73–87.

Matev, K. (2011), Contraintes GPS sur la tectonique actuelle du sud-ouest de la Bulgarie, de la grèce du nord et de l'Albanie, PhD thesis, Université de Grenoble.
Meade, B. J. (2007), Present-day kinematics at the India-Asia collision zone, *Geology*, *35*(1), 81–84.
Molinari, I., and A. Morelli (2011), Epcrust: A reference crustal model for the European Plate, *Geophys. J. Int.*, *185*(1), 352–364.
Molnar, P. (1988), Continental tectonics in the aftermath of plate tectonics, *Nature*, *335*(6186), 131–137.
Molnar, P., and H. Lyon-Caen (1988), Some simple physical aspects of the support, structure, and evolution of mountain belts, *Geol. Soc. Am. Spec. Pap.*, *218*, 179–208.
Molnar, P., and P. Tapponnier (1975), Cenozoic tectonics of Asia: Effects of a continental collision, *Science*, *189*(4201), 419–426.
Nocquet, J.-M. (2012), Present-day kinematics of the Mediterranean: A comprehensive overview of GPS results, *Tectonophysics*, *579*, 220–242.
Nyst, M., and W. Thatcher (2004), New constraints on the active tectonic deformation of the Aegean, *J. Geophys. Res.*, *109*, B11406, doi:10.1029/2003JB002830.
Olive, J.-A., F. Pearce, S. Rondenay, and M. D. Behn (2014), Pronounced zonation of seismic anisotropy in the western Hellenic subduction zone and its geodynamic significance, *Earth Planet. Sci. Lett.*, *391*, 100–109.
Paul, A., H. Karabulut, A. K. Mutlu, and G. Salaün (2014), A comprehensive and densely sampled map of shear-wave azimuthal anisotropy in the Aegean-Anatolia region, *Earth Planet. Sci. Lett.*, *389*, 14–22.
Perouse, E., N. Chamot-Rooke, A. Rabaute, P. Briole, F. Jouanne, I. Georgiev, and D. Dimitrov (2012), Bridging onshore and offshore present-day kinematics of central and eastern Mediterranean: Implications for crustal dynamics and mantle flow, *Geochem. Geophys. Geosyst.*, *13*, Q09013, doi:10.1029/2012GC004289.
Petrovski, J. T. (2004), *Damaging Effects of July 26, 1963 Skopje Earthquake*, Middle East Seismological Forum, Cyber Journal of Geoscience Volume Two.
Picha, F. J. (2002), Late orogenic strike-slip faulting and escape tectonics in frontal Dinarides-Hellenides, Croatia, Yugoslavia, Albania, and Greece, *Bull. Am. Assoc. Petrol. Geol.*, *86*(9), 1659–1671.
Piromallo, C., and A. Morelli (2003), *P* wave tomography of the mantle under the Alpine-Mediterranean area, *J. Geophys. Res.*, *108*(B2), 2065, doi:10.1029/2002JB001757.
Pondrelli, S., S. Salimbeni, G. Ekström, A. Morelli, P. Gasperini, and G. Vannucci (2006), The Italian CMT dataset from 1977 to the present, *Phys. Earth Planet. Inter.*, *159*(3), 286–303.
Pondrelli, S., S. Salimbeni, A. Morelli, G. Ekström, L. Postpischl, G. Vannucci, and E. Boschi (2011), European-Mediterranean regional centroid moment tensor catalog: Solutions for 2005–2008, *Phys. Earth Planet. Inter.*, *185*(3), 74–81.
Ratschbacher, L., W. Frisch, H.-G. Linzer, and O. Merle (1991), Lateral extrusion in the Eastern Alps, part 2: Structural analysis, *Tectonics*, *10*(2), 257–271.
Rebischung, P., J. Griffiths, J. Ray, R. Schmid, X. Collilieux, and B. Garayt (2012), IGS08: The IGS realization of ITRF2008, *GPS Sol.*, *16*(4), 483–494.
Reilinger, R., S. McClusky, D. Paradissis, S. Ergintav, and P. Vernant (2010), Geodetic constraints on the tectonic evolution of the Aegean region and strain accumulation along the Hellenic subduction zone, *Tectonophysics*, *488*(1), 22–30.
Robl, J., and K. Stüwe (2005), Continental collision with finite indenter strength: 2. European Eastern Alps, *Tectonics*, *24*, TC4014, doi:10.1029/2004TC001741.
Royden, L. H., and D. J. Papanikolaou (2011), Slab segmentation and late cenozoic disruption of the Hellenic arc, *Geochem. Geophys. Geosyst.*, *12*, Q03010, doi:10.1029/2010GC003280.
Scherneck, H. (1991), A parametrized solid earth tide model and ocean tide loading effects for global geodetic baseline measurements, *Geophys. J. Int.*, *106*(3), 677–694.
Selverstone, J. (2004), Are the Alps collapsing?, *Annu. Rev. Earth Planet. Sci.*, *33*(1), 113–132.
Serpelloni, E., M. Anzidei, P. Baldi, G. Casula, and A. Galvani (2005), Crustal velocity and strain-rate fields in Italy and surrounding regions: New results from the analysis of permanent and non-permanent GPS networks, *Geophys. J. Int.*, *161*(3), 861–880.
Shanov, S., and N. Dobrev (2000), Tectonic stress field in the epicentral area of 04.04. 1904 Krupnik earthquake from striae on slickensides, in *Reports on Geodesy, Warsaw University of Technology*, vol. 4, pp. 117–122.
Sonder, L. J., and P. England (1986), Vertical averages of rheology of the continental lithosphere: Relation to thin sheet parameters, *Earth Planet. Sci. Lett.*, *77*(1), 81–90.
Speranza, F., I. Islami, C. Kissel, and A. Hyseni (1995), Paleomagnetic evidence for Cenozoic clockwise rotation of the external Albanides, *Earth Planet. Sci. Lett.*, *129*(1), 121–134.
Suckale, J., S. Rondenay, M. Sachpazi, M. Charalampakis, A. Hosa, and L. Royden (2009), High-resolution seismic imaging of the western Hellenic subduction zone using teleseismic scattered waves, *Geophys. J. Int.*, *178*(2), 775–791.
Thatcher, W. (2007), Microplate model for the present-day deformation of Tibet, *J. Geophys. Res.*, *112*, B01401, doi:10.1029/2005JB004244.
Thatcher, W. (2009), How the continents deform: The evidence from tectonic geodesy*, *Annu. Rev. Earth Planet. Sci.*, *37*, 237–262.
Van Hinsbergen, D., C. Langereis, and J. Meulenkamp (2005), Revision of the timing, magnitude and distribution of Neogene rotations in the western Aegean region, *Tectonophysics*, *396*(1), 1–34.
Velaj, T. (2001), Evaporites in Albania and their impact on the thrusting processes, *J. Balkan Geophys. Soc.*, *4*(1), 9–18.
Vergnolle, M., E. Calais, and L. Dong (2007), Dynamics of continental deformation in Asia, *J. Geophys. Res.*, *112*, B11403, doi:10.1029/2006JB004807.
Vrabec, M., and L. Fodor (2006), *Late Cenozoic Tectonics of Slovenia: Structural Styles at the Northeastern Corner of the Adriatic Microplate*, Springer, Netherlands.
Wdowinski, S., Y. Bock, J. Zhang, P. Fang, and J. Genrich (1997), Southern California permanent GPS geodetic array: Spatial filtering of daily positions for estimating coseismic and postseismic displacements induced by the 1992 Landers earthquake, *J. Geophys. Res.*, *102*(B8), 18,057–18,070.
Williams, S. D. (2008), CATS: GPS coordinate time series analysis software, *GPS Sol.*, *12*(2), 147–153.
Willingshofer, E., and S. Cloetingh (2003), Present-day lithospheric strength of the Eastern Alps and its relationship to neotectonics, *Tectonics*, *22*(6), 1075, doi:10.1029/2002TC001463.
Wüstefeld, A., G. Bokelmann, G. Barruol, and J.-P. Montagner (2009), Identifying global seismic anisotropy patterns by correlating shear-wave splitting and surface-wave data, *Phys. Earth Planet. Inter.*, *176*(3), 198–212.
Zumberge, J., M. Heflin, D. Jefferson, M. Watkins, and F. Webb (1997), Precise point positioning for the efficient and robust analysis of GPS data from large networks, *J. Geophys. Res.*, *102*(B3), 5005–5017.